SUPPORTING INFORMATION

Catalytic CO_2 reduction to valuable chemicals using NiFe-based nanoclusters: A first-principle theoretical evaluation

Li Gong[a], Jie-Jie Chen[a], Yang Mu[a,b]*

[a]CAS Key Laboratory of Urban Pollutant Conversion, Collaborative Innovation Centre of Suzhou Nano Science and Technology, Department of Chemistry, University of Science and Technology of China, Hefei, China

[b]Anhui Province Key Laboratory of Polar Environment and Global Change, University of Science and Technology of China, Hefei, China

***Corresponding author:**

Prof. Yang Mu, Fax: +86 551 63607907, E-mail: yangmu@ustc.edu.cn

Table S1 Binding energy ($E_{co\text{-}ads}$) of H_2 and HCO_3^- coadsorption on $Ni@Ni_{11}Fe$ and $Fe@Ni_{12}$ nanoclusters shown in Fig. 2

System	$E_{co\text{-}ads}$ (eV)
a	-2.61
b	-2.96
c	-2.64
d	-4.60

Table S2 Calculated total energies (*E*), zero-point energies (*ZPE*), entropies (*S*) multiplied by temperature (T =298.15 K) (*TS*), and free energies (*G*) of intermediates in HCO_3^- reduction process on $Ni@Ni_{11}Fe$ and $Fe@Ni_{12}$ nanoclusters

Intermediate	$Ni@Ni_{11}Fe$				$Fe@Ni_{12}$			
	ZPE (eV)	*TS* (eV)	*E* (eV)	*G* (eV)	*ZPE* (eV)	*TS* (eV)	*E* (eV)	*G* (eV)
State 1	1.67	1.19	-18611.33	-18610.85	1.58	1.26	-18609.91	-18609.59
State 2	1.86	1.14	-18614.40	-18613.67	1.96	1.13	-18613.24	-18612.41
State 3	1.78	0.97	-18613.27	-18612.45	1.63	1.06	-18612.43	-18611.86
State 4	2.07	1.16	-18614.25	-18613.33	1.86	1.06	-18613.06	-18612.26
State 5	1.84	1.42	-18612.38	-18611.96	1.89	0.96	-18611.02	-18610.08
State 6	1.76	1.29	-18612.61	-18612.15	1.97	1.06	-18611.49	-18610.57
State 7	1.69	0.77	-18614.58	-18613.66	2.00	1.15	-18612.81	-18611.97
State 8	1.91	1.16	-18613.20	-18612.45	1.78	1.17	-18609.27	-18608.66

Table S3 Calculated thermodynamic properties (ΔG) and energy barrier (E_a) in HCO_3^- reduction process on $Ni@Ni_{11}Fe$ and $Fe@Ni_{12}$ nanoclusters at 298.15 K and 1 atm

Pathway	Step	$Ni@Ni_{11}Fe$		$Fe@Ni_{12}$	
		ΔG (eV)	E_a (eV)	ΔG(eV)	E_a (eV)
1	1→2	-2.82	-0.09	-2.82	-0.01
	2→3	1.22	1.61	0.55	0.94
	3→4	-0.88	–	-0.4	–
2	1→2	-2.82	-0.09	-2.82	-0.01
	2→5	1.71	2.70	2.32	2.19
	5→6	-0.19	–	-0.49	–
	6→4	-1.18	–	-1.69	–
3	1→2	-2.82	-0.09	-2.82	-0.01
	2→7	0.01	2.50	0.44	2.72
	7→8	1.21	1.68	3.31	0.77

Table S4 Binding energy (E_{ads}) of $HCOO^-$ adsorption on$Ni@Ni_{11}Fe$, $Fe@Ni_{12}$ and Ni_{13} nanoclusters shown in Fig. S3

System	E_{ads} (eV)
a	-1.71
b	-2.42
c	-1.39
d	-1.72
e	-2.40
f	-2.46
g	-1.47
h	-2.27

Table S5 Calculated thermodynamic properties (ΔG) and energy barrier (E_a) in formic acid ($HCOO^{-*}$) reduction to formaldehyde (CHO^{-*}) process in aqueous system on $Ni@Ni_{11}Fe$, $Fe@Ni_{12}$ and Ni_{13} at 298.15 K and 1 atm

Step	$Ni@Ni_{11}Fe$		$Fe@Ni_{12}$		Ni_{13}	
	ΔG (eV)	E_a (eV)	ΔG (eV)	E_a (eV)	ΔG (eV)	E_a (eV)
$HCOO^{-*} + H^* \rightarrow HCOOH^* + e^-$	2.55	2.62	1.93	2.67	1.75	2.52
$(HCOOH^* + e^-) + H^* \rightarrow CHO^{-*} + H_2O$	-1.06	1.20	1.30	2.08	0.79	3.10
Total	1.49	–	3.23	–	2.45	–

Table S6 Binding energy (E_{ads}) of $Ni@Ni_{11}Fe$ and $Fe@Ni_{12}$ nanoclusters adsorption on graphene shown in Fig. 6 (G for graphene)

System	E_{ads} (eV)
$Ni@Ni_{11}Fe$/G-1	-2.23
$Ni@Ni_{11}Fe$/G-2	-2.22
$Fe@Ni_{12}$/G-1	-0.10
$Fe@Ni_{12}$/G-2	-1.86
$Fe@Ni_{12}$/G-3	-1.56
$Fe@Ni_{12}$/G-4	-3.01

Table S7 Binding energy (E_{ads}) of H_2 adsorption on graphene supported $Ni@Ni_{11}Fe$ and $Fe@Ni_{12}$ nanoclusters. The H_2 adsorption configuration on graphene supported $Ni@Ni_{11}Fe$ and $Fe@Ni_{12}$ nanoclusters were similar to the ones $Ni@Ni_{11}Fe$ and $Fe@Ni_{12}$ nanoclusters shown in Figure 1 (t for molecules top on nanocluster, b for molecules bridge on nanocluster, and G for graphene)

System	E_{ads} (eV)
H_2-$Ni@Ni_{11}Fe$/G-1)-t_1	0.77
H_2-($Ni@Ni_{11}Fe$/G-1)-t_2	0.73
H_2-($Ni@Ni_{11}Fe$/G-1)-b	-0.16
H_2-($Fe@Ni_{12}$/G-2)-t_1	-0.74
H_2-($Fe@Ni_{12}$/G-2)-t_2	-0.88
H_2-($Fe@Ni_{12}$/G-2)-b_1	-1.05
H_2-($Fe@Ni_{12}$/G-4)-b_2	-0.35
H_2-($Fe@Ni_{12}$/G-4)-t_1	0.32
H_2-($Fe@Ni_{12}$/G-4)-t_2	1.11
H_2-($Fe@Ni_{12}$/G-4)-b	-0.31

Table S8 Binding energy (E_{ads}) of HCO_2^- adsorption on graphene supported Ni@Ni_{11}Fe and Fe@Ni_{12} nanoclusters, shown in Figure S4 (t for molecules top on nanocluster, b for molecules bridge on nanocluster, and G for graphene)

System	E_{ads} (eV)
HCO_2^--(Ni@Ni_{11}Fe/G-1)-t	3.19
HCO_2^--(Ni@Ni_{11}Fe/G-1)-b	2.05
HCO_2-(Fe@Ni_{12}/G-2)-t_1	1.70
HCO_2-(Fe@Ni_{12}/G-2)-t_2	0.98
HCO_2-(Fe@Ni_{12}/G-2)-b_1	0.06
HCO_2-(Fe@Ni_{12}/G-2)-b_2	0.77
HCO_2^--(Fe@Ni_{12}/G-4)-t	–
HCO_2^--(Fe@Ni_{12}/G-4)-b	0.43

Table S9 Calculated thermodynamic properties (ΔG) and energy barrier (E_a) in formic acid ($HCOO^{-*}$) reduction to formaldehyde (CHO^{-*}) process in aqueous system on graphene supported $Ni@Ni_{11}Fe$ and $Fe@Ni_{12}$ nanoclusters at 298.15 K and 1 atm

Step	graphene supported $Ni@Ni_{11}Fe$		graphene supported $Fe@Ni_{12}$	
	ΔG (eV)	E_a (eV)	ΔG (eV)	E_a (eV)
$HCOO^{-*} + H^* \rightarrow HCOOH^* + e^-$	-1.40	0.12	0.54	1.61
$(HCOOH^* + e^-) + H^* \rightarrow CHO^{-*} + H_2O$	2.57	4.20	2.12	4.34
Total	1.17	–	2.66	–

Figure Legends

Fig. S1 Geometry optimized adsorption structures of H_2 on $Ni@Ni_{11}Fe$ and $Fe@Ni_{12}$ nanoclusters.

Fig. S2 Geometry optimized adsorption structures of HCO_3^- on different nanoclusters: a and b for $Ni@Ni_{11}Fe$ nanocluster, and c-f for $Fe@Ni_{12}$ nanocluster.

Fig. S3 Geometry optimized adsorption structures of $HCOO^-$ on various nanoclusters: a and b for $Ni@Ni_{11}Fe$ nanocluster, and c-f for $Fe@Ni_{12}$ nanocluster, and g and h for Ni_{13} nanocluster.

Fig. S4 Geometry optimized adsorption structures of $HCOO^-$ on graphene supported $Ni@Ni_{11}Fe$ and $Fe@Ni_{12}$ nanoclusters.

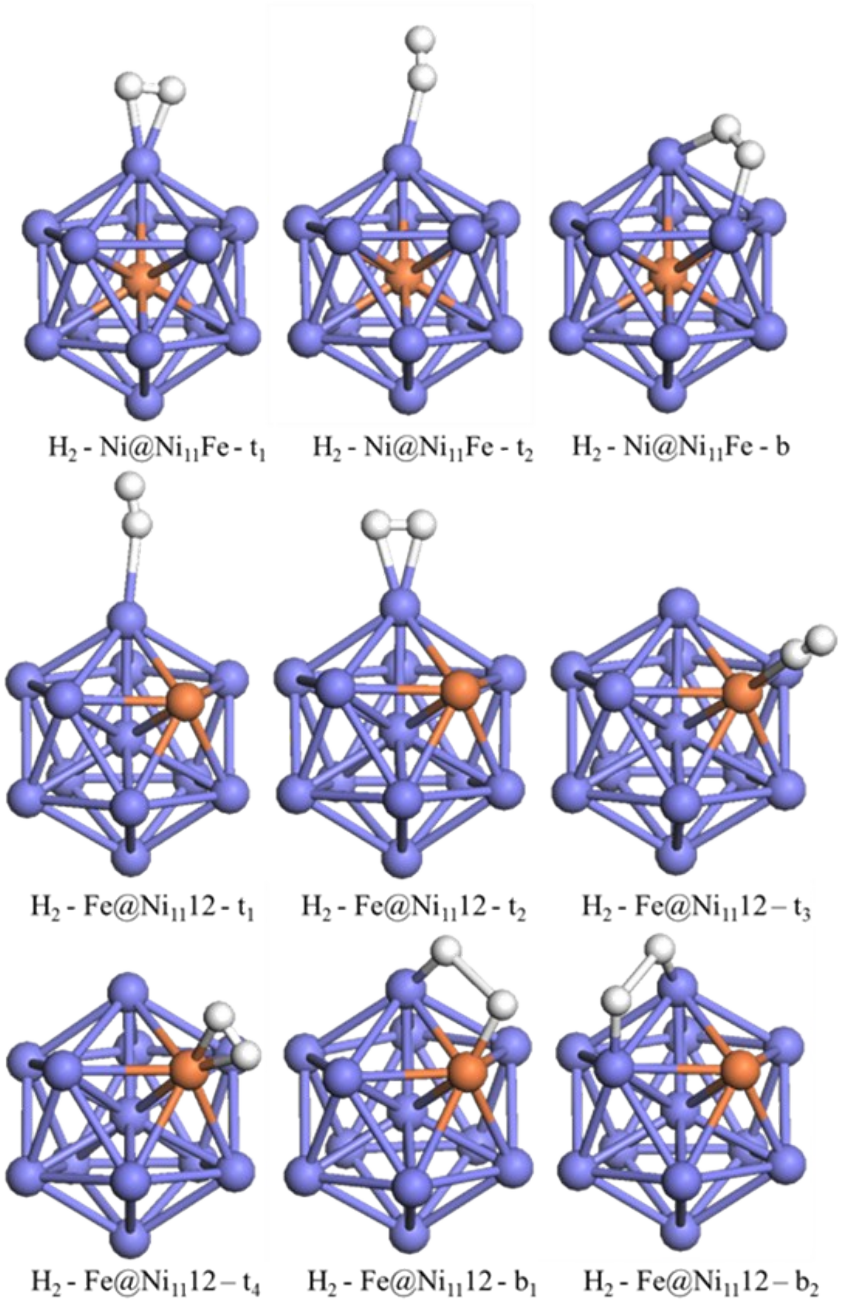
H_2 - Ni@Ni_{11}Fe - t_1
H_2 - Ni@Ni_{11}Fe - t_2
H_2 - Ni@Ni_{11}Fe - b
H_2 - Fe@Ni_{11}12 - t_1
H_2 - Fe@Ni_{11}12 - t_2
H_2 - Fe@Ni_{11}12 – t_3
H_2 - Fe@Ni_{11}12 – t_4
H_2 - Fe@Ni_{11}12 - b_1
H_2 - Fe@Ni_{11}12 – b_2

Fig. S1

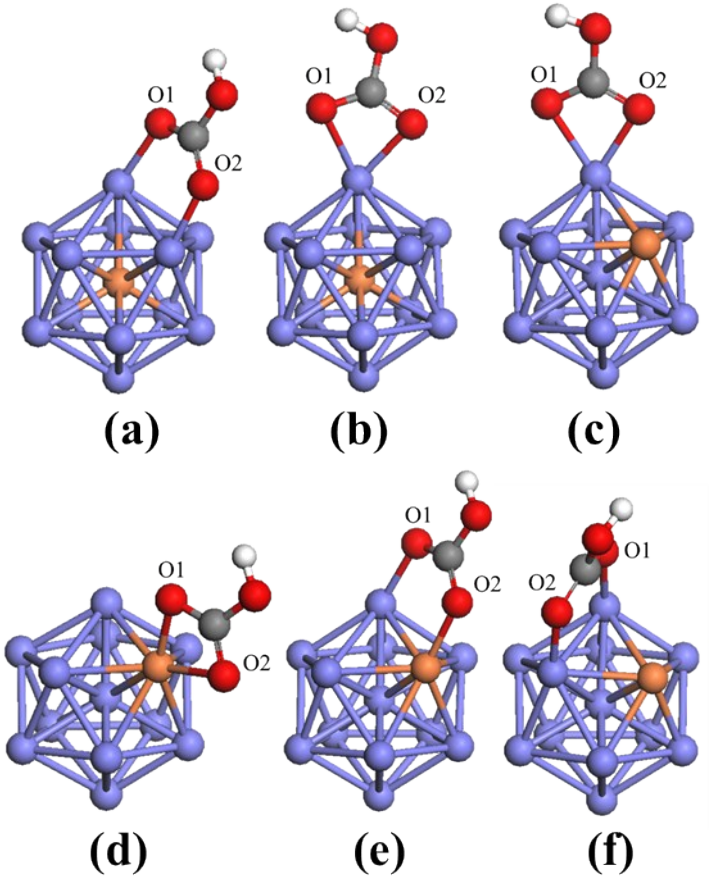

85

86

87 **Fig. S2**

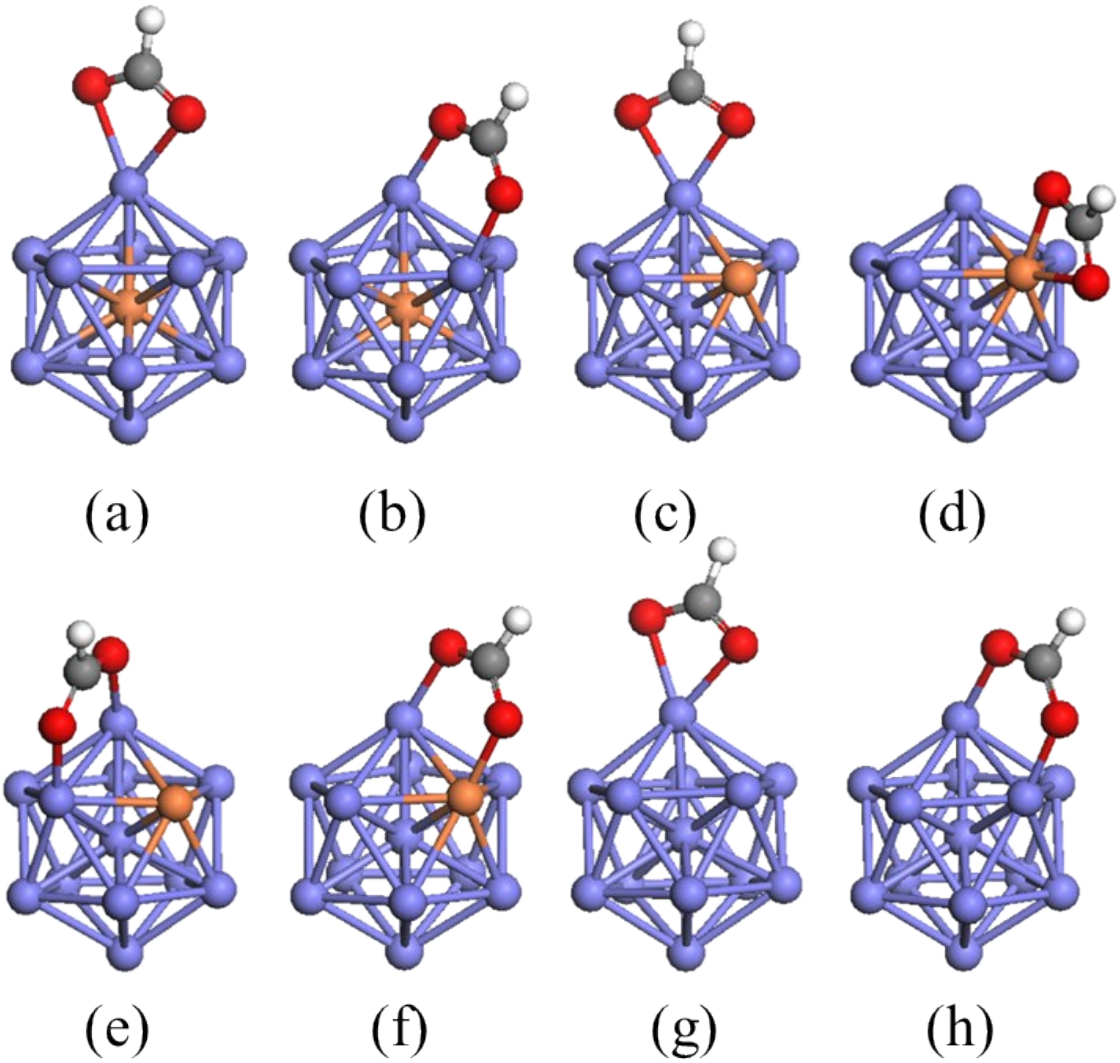

Fig. S3

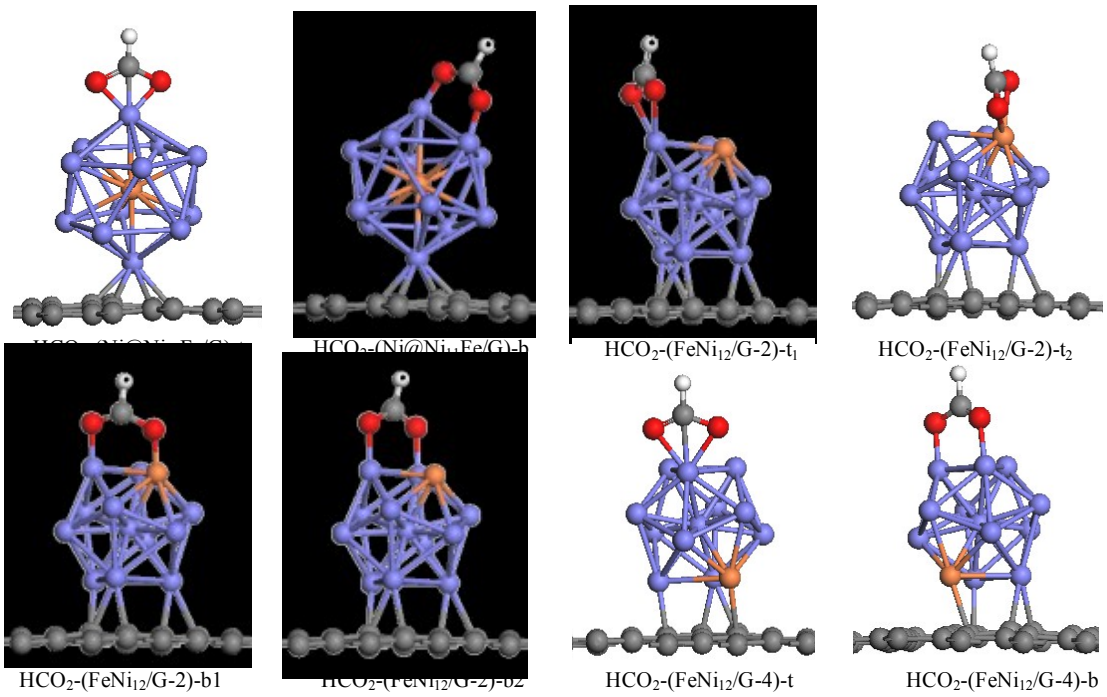

92

93

94 **Fig. S4**

95

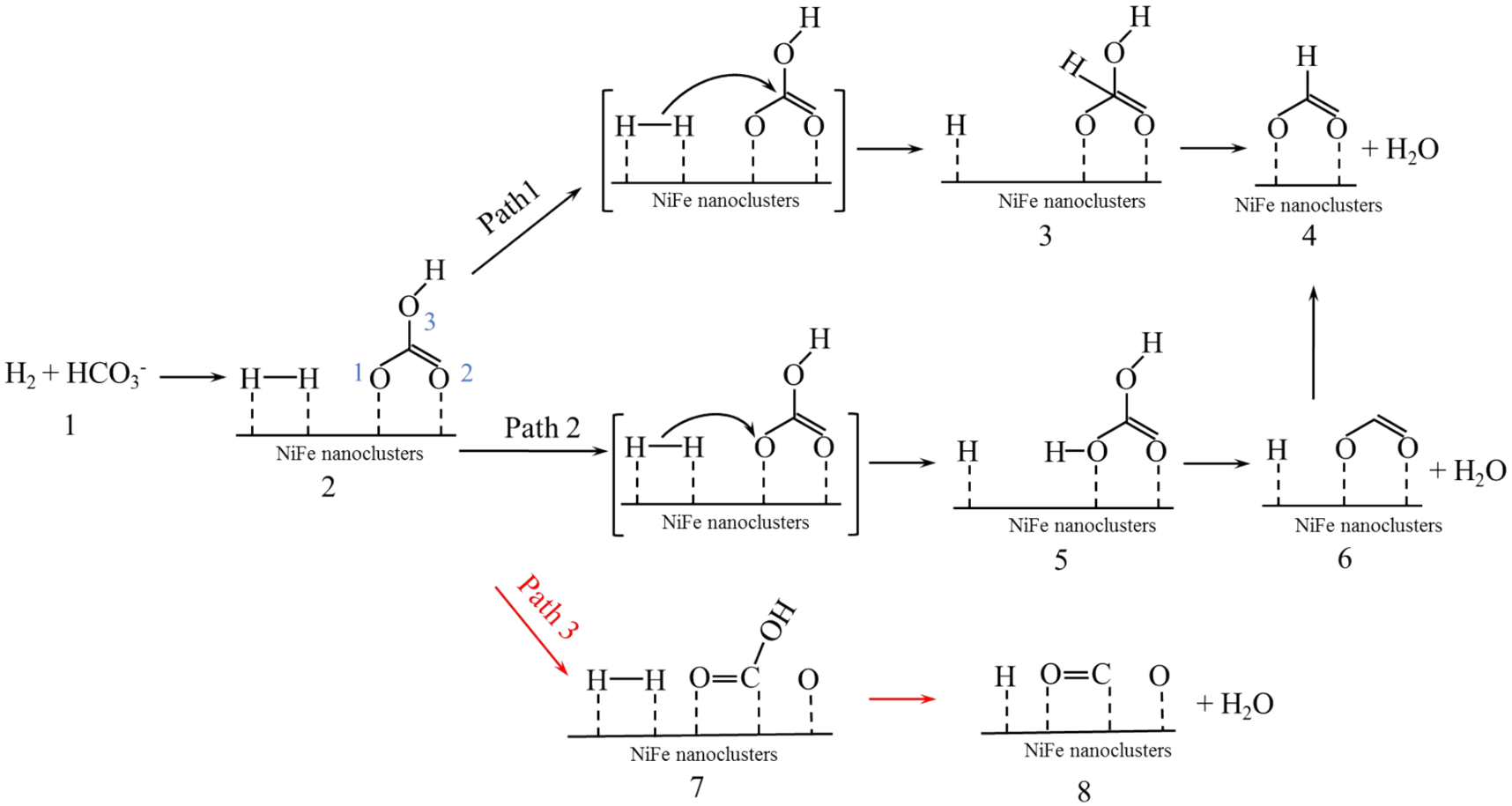

96

97 **Scheme S1** Reaction pathways of HCO_3^- reduction to $HCOO^-$ and CO formation on $Ni@Ni_{11}Fe$ and $Fe@Ni_{12}$ nanoclusters.

$$HCOO^{-*} \xrightarrow{+H^*} HCOOH^* + e^- \xrightarrow{+H^*} CHO^{-*} + H_2O$$

Scheme S2 Proposed mechanism for adsorbed formic acid ($HCOO^{-*}$) reduction to formaldehyde (HCO^{-*}) on $Ni@Ni_{11}Fe$, $Fe@Ni_{12}$ and Ni_{13} nanoclusters in aqueous solution.